Am J Physiol Gastrointest Liver Physiol 297: G1041–G1052, 2009.
First published October 15, 2009; doi:10.1152/ajpgi.00328.2009.

TRANSLATIONAL PHYSIOLOGY

Oral PEG 15–20 protects the intestine against radiation: role of lipid rafts

Vesta Valuckaite,*[1,2] Olga Zaborina,*[2] Jason Long,*[2] Martin Hauer-Jensen,[7] Junru Wang,[7] Christopher Holbrook,[2] Alexander Zaborin,[2] Kenneth Drabik,[3] Mukta Katdare,[4] Helena Mauceri,[4] Ralph Weichselbaum,[4] Millicent A. Firestone,[1,5] Ka Yee Lee,[6] Eugene B. Chang,[3] Jeffrey Matthews,[1,2] and John C. Alverdy[1,2]

[1]*Bioengineering Institute for Advanced Surgery and Endoscopy (BIASE), Departments of* [2]*Surgery,* [3]*Medicine, and* [4]*Radiation Oncology, Pritzker School of Medicine, and* [6]*Institute for Biophysical Dynamics, the James Franck Institute, University of Chicago, Chicago, Illinois;* [5]*Materials Science Division, Argonne National Laboratory, Argonne, Illinois;* [7]*Department of Pharmaceutical Sciences, University of Arkansas for Medical Sciences and Surgical Service, Central Arkansas Veterans Healthcare System, Little Rock, Arkansas*

Submitted 5 August 2009; accepted in final form 8 October 2009

Valuckaite V, Zaborina O, Long J, Hauer-Jensen M, Wang J, Holbrook C, Zaborin A, Drabik K, Katdare M, Mauceri H, Weichselbaum R, Firestone MA, Lee KY, Chang EB, Matthews J, Alverdy JC. Oral PEG 15–20 protects the intestine against radiation: role of lipid rafts. *Am J Physiol Gastrointest Liver Physiol* 297: G1041–G1052, 2009. First published October 15, 2009; doi:10.1152/ajpgi.00328.2009.—Intestinal injury following abdominal radiation therapy or accidental exposure remains a significant clinical problem that can result in varying degrees of mucosal destruction such as ulceration, vascular sclerosis, intestinal wall fibrosis, loss of barrier function, and even lethal gut-derived sepsis. We determined the ability of a high-molecular-weight polyethylene glycol-based copolymer, PEG 15–20, to protect the intestine against the early and late effects of radiation in mice and rats and to determine its mechanism of action by examining cultured rat intestinal epithelia. Rats were exposed to fractionated radiation in an established model of intestinal injury, whereby an intestinal segment is surgically placed into the scrotum and radiated daily. Radiation injury score was decreased in a dose-dependent manner in rats gavaged with 0.5 or 2.0 g/kg per day of PEG 15–20 ($n = 9$–13/group, $P < 0.005$). Complementary studies were performed in a novel mouse model of abdominal radiation followed by intestinal inoculation with *Pseudomonas aeruginosa* (*P. aeruginosa*), a common pathogen that causes lethal gut-derived sepsis following radiation. Mice mortality was decreased by 40% in mice drinking 1% PEG 15–20 ($n = 10$/group, $P < 0.001$). Parallel studies were performed in cultured rat intestinal epithelial cells treated with PEG 15–20 before radiation. Results demonstrated that PEG 15–20 prevented radiation-induced intestinal injury in rats, prevented apoptosis and lethal sepsis attributable to *P. aeruginosa* in mice, and protected cultured intestinal epithelial cells from apoptosis and microbial adherence and possible invasion. PEG 15–20 appeared to exert its protective effect via its binding to lipid rafts by preventing their coalescence, a hallmark feature in intestinal epithelial cells exposed to radiation.

Pseudomonas aeruginosa; gut-derived sepsis; apoptosis; radiation injury

TRANSLATIONAL HIGHLIGHTS Effective and safe measures to protect the intestine against radiation injury following medical therapy or accidental exposure remain a challenge and often limit the use of radiation to cure malignancy. This study demonstrated that, in rodents, oral administration of high-molecular-weight polyethylene glycol (PEG 15–20) protects the intestine following radiation exposure and reduces the secondary effects of sepsis from intestinal pathogens. Protective mechanisms involve modulation of lipid rafts and suppression of bacterial virulence gene activation. The safety profile, intestinal distribution dynamics, and ease of delivery of PEG 15–20 make it highly suitable for clinical testing.

The precise mechanism(s) by which abdominal radiation causes epithelial cell damage and inflammation, loss of intestinal barrier function, and lethal sepsis is complex. These effects often limit the deliverable dose of radiation for the treatment of abdominal and pelvic malignancies. Acute intestinal radiation injury is characterized by intestinal epithelial cell (IEC) apoptosis, epithelial barrier breakdown, mucosal inflammation, late-onset vascular sclerosis, and intestinal wall fibrosis (32, 36, 46). Ionizing radiation is also known to enhance the susceptibility of the host to systemic infections attributable to endogenous and exogenous organisms (7). Among gut-derived infections, *Pseudomonas aeruginosa* (*P. aeruginosa*) appears to be particularly prevalent and is often lethal following both clinical and experimental radiation exposure (4, 5, 16). Although it is assumed that this higher mortality rate is attributable to dissemination of the organism across the damaged mucosa (4, 5), failure to isolate the organism in extraintestinal sites (i.e., blood, tissues) in a manner that correlates to mortality (13) suggests that *P. aeruginosa* may act locally with the intestinal mucosa itself to cause systemic sepsis (26). These observations, coupled with the finding that germ-free mice have enhanced survival following radiation exposure, provide compelling evidence that the intestinal microbial flora play a critical role in radiation-associated mortality beyond their ability to disseminate (9, 41).

Despite these insights, the precise pathogenesis of the intestinal radiation syndrome remains controversial. Some authors consider the formation of free radicals during exposure to radiation to be important in the production of intestinal damage, forming the bases for the use of endogenous and exogenous thiol compounds, which act as free-radical scavengers (43). Others assert that the primary lesion following radiation is confined to the microvascular endothelium, after which there is leakage of a circulating factor by a bystander effect that

* V. Valuckaite, O. Zaborina, and J. Long contributed equally to this work.
Address for reprint requests and other correspondence: J. Alverdy, FACS, Prof. of Surgery, Director, Center for Surgical Infection Research, Univ. of Chicago, Pritzker School of Medicine, 5841 S. Maryland MC 6090 Chicago, IL 60637 (e-mail: jalverdy@surgery.bsd.uchicago.edu).

regulates the stem cell response to radiation (33). Because it is likely that there are multiple effects of radiation on various compartments, cells, and signaling pathways within the intestinal tract and its microflora, therapies that can target the multicellular nature of this complex organ are most likely to be effective. Polyethylene glycols (PEGs) are a group of compounds that, depending on their molecular weight and structural conformation, can anchor to living surfaces and shield against bacterial adhesion, in essence behaving as surrogate mucins or eukaryotic biofilms on the intestinal epithelium (48, 52). PEG compounds have been described as biologically inert and nonmicrobiocidal (52). However, these compounds can directly affect membrane function across a wide variety of cell types and injuries, resulting in prevention of loss of function and even recovery of injured tissues (23, 31, 35).

We have previously reported that a nonabsorbed high-molecular-weight PEG copolymer (PEG 15–20) can prevent the adherence and possible invasion of *P. aeruginosa* to the intestinal epithelium, preserve intestinal barrier function, and prevent mortality in a mouse model of lethal gut-derived sepsis attributable to intestinal *P. aeruginosa* (52). We had screened a large library of PEG compounds using in vitro IEC culture experiments and mice and identified that PEG 15–20 demonstrated unique tolerability (no change in cell or animal growth, no diarrhea) and that PEG 15–20 exerted potent intestinal protective properties compared with lower-molecular-weight or simple-linear noncopolymeric derivatives.

In the present study, we tested the ability of orally delivered PEG 15–20 to prevent intestinal injury and sepsis in animals following radiation exposure and found a protective action of the compound against both intestinal radiation injury and lethal gut-derived sepsis. We performed complementary in vitro experiments using cultured IECs and determined that PEG 15–20 may exert its protective effect by associating with lipid rafts and preventing their coalescence. PEG-15–20 also attenuated virulence expression in *P. aeruginosa* in response to secreted products from cultured IECs exposed to radiation and physically distanced *P. aeruginosa* away from the epithelial cell surface. Taken together, these studies provide compelling evidence that oral PEG 15–20 might function as an intestinal radioprotectant not only by affecting epithelial membrane lipid raft function but also by interdicting in the host pathogen response to radiation exposure.

MATERIALS AND METHODS

Bacterial strains. P. aeruginosa strains PAO1 and its derivative strain PAO1/enhanced green fluorescent protein (EGFP) harboring the *egfp* gene encoding green fluorescent protein EGFP on the pUCP24 plasmid vector expressed under *Plac* promoter (52) were used. This strain constitutively expresses GFP-facilitating localization of *P. aeruginosa*. In addition the PA-I lectin/adhesin luminescent reporter strain PAO1/*lecA::lux* (50) was used in selected experiments. The luminescent PA-I reporter strain shows the expression of the PA-I lectin, a barrier-dysregulating protein that we have previously shown to be a key virulence factor in lethal gut-derived sepsis attributable to *P. aeruginosa* (29). The PA-I lectin alters intestinal tight junctional proteins and facilitates permeation of lethal toxins of this organism into the systemic compartment.

Epithelial cell lines. Rat IECs (IEC-18 cells, *passages 30-34*) were used in all experiments. IEC-18 cells were routinely cultured in plastic culture flasks containing DMEM media (DMEM, high glucose, 4.5 g/l containing 5% heat-inactivated fetal bovine serum and 0.1 U/ml insulin).

High-molecular-weight PEG 15–20. High-molecular-weight PEG 15,000–20,000 Da (catalog no. P2263), referred to as PEG 15–20, was purchased from Sigma (St. Louis, MO). For imaging studies, the nascent PEG 15–20 was fused with fluorescein as custom prepared by Sigma (batch 478–004-2, 28-Nov-06) and visualized using the Xenogen in vivo imaging system.

Localized, fractionated irradiation of rat small intestine. Under experimental protocols, approved by the University of Arkansas for Medical Sciences Institutional Animal Care and Use Committee, a total of 37 male Sprague-Dawley rats, 43–49 days of age (175–200 g; Harlan, Indianapolis, IN), were used for these experiments. The surgical model for localized small bowel irradiation was used, as described previously (17). Briefly, rats underwent bilateral orchiectomy, and a loop of distal ileum in continuity with the rest of the bowel was sutured to the inside of the left part of the empty scrotum. After 3-wk postoperative recovery, the rats were randomly assigned to three groups: control (autoclaved distilled water), PEG 15–20 (0.5 g/kg per day), or PEG 15–20 (2 g/kg per day) that was delivered by daily oral gavage (average gavage volume 2.5 ml) with a 16-gauge curved gavage needle (Cadence Science, Lake Success, NY) from 3 days before the start of radiation, during irradiation (9 day), and for 14 days thereafter. The rats were anesthetized with isoflurane inhalation during irradiation. The transposed bowel segment within the "scrotal hernia" was exposed to once daily 5.0 Gy-fractionated irradiation for 9 consecutive days (no weekend break). Irradiation was delivered by a Seifert Isovolt 320 X-ray machine (Seifert X-Ray, Fairview Village, PA), operated at 250 kVp and 15 mA, with 3 mm Al-added filtration (half-value layer 0.85 mm Cu, dose rate 4.49 Gy/min). The rats were euthanized 2 wk after the completion of the fractionated radiation schedule. This time point represents the early (subacute) stage in radiation enteropathy development in our model system (17, 28). Specimens of irradiated and unirradiated intestine were procured and fixed in methanol-Carnoy's solution for histological and morphometric/stereological analysis.

The overall severity of structural radiation injury was assessed using the radiation injury score (RIS) scoring system. The RIS is a composite histopathological scoring system that provides a global measure of structural radiation injury (22, 28). Briefly, seven histopathological parameters of radiation injury (mucosal ulcerations, epithelial atypia, thickening of subserosa, vascular sclerosis, intestinal wall fibrosis, ileitis cystica profunda, and lymph congestion) were graded from 0–3. The sum of the scores for the individual alterations constitutes the RIS. All specimens were evaluated in a blinded fashion by two separate researchers, and discrepancies in scores were resolved by consensus. Mucosal surface area was measured in vertical sections using the stereological projection/cycloid method described by Baddeley (1), adapted to our model system (27). Intestinal wall thickness (submucosa, muscularis externa, and subserosa) and subserosal thickness were measured with a ×10 objective and computer-assisted image analysis (Image-Pro Plus; Media Cybernetics, Silver Spring, MD). In each of five areas, 500 μm apart, three vertical lines were drawn, centered in the left, middle, and right third.

Mouse model of postabdominal radiation gut-derived sepsis induced by P. aeruginosa. Under IACUC protocols 70931 and 71744, 8-wk-old male C57BL6 mice ($n = 10$/group) were fasted 12 h before a single dose of 13 Gy abdominal irradiation delivered from an X-ray generated irradiator. Preliminary experiments performed using various doses of abdominal radiation demonstrated a 0–20% mortality at 13 Gy, similar to other published reports (34). This dose was chosen for all subsequent experiments to allow for the synergistic effect of intestinal *P. aeruginosa* in this model to be observed. Following irradiation, all mice continued to fast but were allowed to drink ad libitum either a 5% dextrose solution in water (D5W) (control) or 1% PEG 15–20 solution in D5W for 48 h. All mice drank an average of 2.5–3.0 ml/24 h of solutions. Mice underwent surgical laparotomy

under general anesthesia and were directly inoculated with 200 μl of 10^7 CFU/ml of *P. aeruginosa* PAO1 in a 10% glycerol solution using a 27-gauge syringe via cecal puncture. Groups of mice injected with 200 μl of 10% glycerol served as controls. Postoperatively, both groups of mice were maintained on D5W or 1% PEG 15–20 in water supplemented with 5% dextrose and transitioned to mouse chow diet 24 h later for the remainder of the experiment. All mice were followed and observed twice daily for the development of sepsis. Mice were euthanized when they were frankly septic (lethargy, chromodacctyrhhea, liquid stools, ruffled fur).

In vivo imaging of ingested fluorescein-labeled PEG 15–20. To assess the distribution of PEG in the gastrointestinal tract, 8-wk-old male C57BL6 mice ($n = 3$/group) were allowed to drink fluorescein-labeled PEG 15–20 (Fl-PEG) (1% solution) (IACUC protocol no. 71744) with 5% dextrose. Control mice were given D5W in sterile water. All mice were allowed a normal chow diet during the study period. The Xenogen IVIS 200 in vivo fluorescence imaging system (Optical Imaging Core Facility, University of Chicago) was used to capture daily sequential abdominal images of mice. All mice were anesthetized with intraperitoneal injection of ketamine/xylazine, and their hair was removed with Nair solution to enhance signal sensitivity.

Epithelial cell lines and exposure to radiation. Rat IEC (IEC-18 cells, *passages 30-34*) were used in all experiments. IEC-18 cells were routinely cultured in plastic culture flasks containing DMEM media (DMEM, high glucose, 4.5 g/l containing 5% heat-inactivated fetal bovine serum and 0.1 U/ml insulin). IEC-18 cells were cultivated for 2–3 days before the experiments started. The cells were cultivated in glass-bottom culture dishes p35 (MatTek, Ashland, MA; part no. P35GCol-0–14-C, collagen coated), and the number of cells seeded was $\sim 2 \times 10^5$. After 2–3 days, IEC-18 cells reached confluency. Cells were either grown to 90% confluence (for subsequent irradiation assays) or to complete confluence as a monolayer (for bacterial adhesion assays). Five Gy of radiation was generated from a Co-60 gamma source at a dose rate of 1.27 Gy/min.

Small angle X-ray analysis of PEG 15–20. Small-angle X-ray scattering (SAXS) is a small-angle scattering (SAS) technique where the elastic scattering of X-rays within a sample containing homogeneities in the nm range is recorded at very low angles (typically 0.1–10°). This angular range contains information about the shape and size of macromolecules and characteristic distances of partially ordered materials. SAXS is capable of delivering structural information of macromolecules between 5 and 25 nm and of repeat distances in partially ordered systems of up to 150 nm. Samples for SAXS studies were prepared as quaternary compositions as previously described (11, 12). All samples were prepared such that the polymer-to-phospholipid ratio was held at 2–30 mol%. Hydration of the solid components in deionized water was accomplished by repeated cycles of heating (50°C), vortex mixing, and cooling on an ice bath until sample uniformity was achieved. SAXS measurements were made using the instrument at undulator beamline 12ID-C of the Advanced Photon Source at Argonne National Laboratory.

Atomic force microscopy. Atomic force microscopy (AFM) is a method of measuring surface topography on a scale from angstroms to 100 microns. The technique involves the use of a highly sensitive catalever tip that "taps" at nanoscale units within a radius of 20 nm to record surface-tip interactions. Variations in tip height are recorded, producing a topographic image of the surface. In our experiments, we used a tapping mode AFM performed in air with a Multimode Nanoscope IIIA Scanning Probe Microscope without using an O-ring (MMAFM; Digital Instruments, Woodbury, NY). Intestinal tissue sections (terminal ileum and proximal colon) were harvested from mice ($n = 3$/group) drinking PEG 15–20 solution or tap water ad libitum on a normal chow diet for 1 wk before euthanasia. Sections were opened longitudinally with sharp dissection, placed luminal side up on mica, and imaged with a Multimode Nanoscope IIIA Scanning Probe Microscope.

Cell death and apoptosis assays. A cell death ELISA kit (Cell Death Detection ELISA^{PLUS}; Roche Molecular Biochemicals, Indianapolis, IN) was used to detect apoptosis and necrosis 24 h after irradiation. Cell culture media (conditioned media) was used for the necrosis assay while cells were treated with lysis buffer and used for apoptosis as recommended by the manufacturer. Nuclear DNA fragmentation was detected using the TUNEL assay (In Situ Cell Death Detection Kit, peroxidase, Roche Diagnostics; cat no. 11684817910). Briefly, IEC growth media was discarded, and cells were fixed in 4% formaldehyde, permeabilized in 0.2% Triton X-100, and incubated with TdT incubation buffer for 60 min in a 37°C humidified incubator for 3′-OH labeling. Stained cells were analyzed using fluorescent confocal microscopy.

Cholesterol depletion. For cholesterol depletion, cells were incubated for 60 min at 37°C in DMEM containing 15 mM of methylcyclodextrin (20). Control cells were incubated in the same medium lacking cyclodextrin. Cholesterol depletion was verified by the absence of lipid rafts as assessed by toxin B binding.

TUNEL assay and hematoxylin and eosin staining of intestinal epithelium in mice. Routine 5-μm paraffin sections of mice ilea were prepared. The TUNEL assay was performed using the Apop Tag Plus Peroxidase in Situ Apoptosis Kit (S7107; Millipore, Billerica, MA). The degree of apoptosis was determined by detection of the brown stained area per 10 μm^2 using Automated Cellular Imaging Software. All evaluations were performed by a pathologist in a blinded fashion.

Spatial orientation of P. aeruginosa to IEC-18 cells. Twenty-four hours following radiation, 100 μl of *P. aeruginosa* strain MPAO1/EGFP (10^7 CFU/ml) was added apically on IEC cells as previously described (52). Real-time imaging was performed using laser scanning confocal microscopy (model TCS SP2 AOS; Leica, Manheim, Germany).

Lipid raft coalescence. IEC-18 cells were grown to confluency, and assigned cells were treated for 1 h with 5% PEG 15–20 followed by gentle washing with regular IEC cell media to remove any nonbound PEG. Growth media was changed before irradiation in all groups, and assigned cells were exposed to 5 Gy. At 24 h, assigned cells were apically exposed to *P. aeruginosa* PAO1, 10^7 CFU, for 30 min followed by washing with cell media. Lipid rafts were visualized using the Molecular Probes Vybrant Lipid raft labeling kit. Lipid rafts were visualized by fluorescence microscopy.

Sucrose density gradient. Adherent confluent IEC cells were washed twice in ice-cold PBS and lysed with 2 ml of extraction buffer (20 mM Tris·HCl, pH 7.4, NaCl 150 mM, EDTA 1 mM) supplemented with 1% Triton X-100 and a protease inhibitor mixture. Lysates were scraped from the flasks, sheared by 20 passages through a 22-gauge needle, left for 20 min before mixing with OptiPrep density gradient medium [final concentration, 40% (vol/vol)], and placed at the bottom of a 12-ml ultracentrifuge tube. A discontinuous OptiPrep gradient was formed by overlaying 4 ml of 30% Optiprep and 4 ml of 5% Optiprep (prepared by dilution of OptiPrep in extraction buffer). Gradients were ultracentrifuged at 100,000 *g* for 4 h in a SW41 rotor (Beckman Coulter, Fullerton, CA). A distinct Triton X-100-insoluble whitish band that floated to the 5–30% interface was designated as the detergent-resistant membrane fraction. The whole procedure was performed at 0–4°C, followed by Western blot analysis for the detection of flotillin (cat no. 610820, Purified mouse anti-Flotillin 1- MAb; BD Transduction Laboratories, San Diego, CA), a marker for detergent-resistant membranes.

Statistical analysis. All statistical analyses were performed using Student's *t*-test using Sigma Plot software. Kaplan-Meier Survival analysis was performed using SPSS 15.0 software.

RESULTS

PEG 15–20 attenuates radiation-induced intestinal injury in the fractionated rat scrotal model and prevents radiation-induced apoptosis in cultured rat IECs. In the fractionated rat intestinal scrotal model, control rats demonstrated typical early alterations (2 wk after irradiation) in the intestinal segments

within the scrotum consisting mainly of mucosal injury and ulcerations, reactive bowel wall thickening, pronounced reactive subserosal fibrosis, and inflammatory cell infiltration. PEG 15–20 caused a statistically significant dose-dependent amelioration of all parameters of radiation injury: radiation injury score (Fig. 1*A*), mucosal surface area (Fig. 1*B*), intestinal wall thickening (Fig. 1*C*), and serosal thickening (Fig. 1*D*). PEG 15–20 did not affect any of the parameters of injury in unirradiated (shielded) intestine (data not shown).

PEG 15–20 protected cultured rat intestinal epithelial monolayers (IEC-18) from development of apoptosis according to experiments outlined in Fig. 1*E*. Exposure of IEC-18 cells to 5% PEG 15–20 for 1 h resulted in attenuation of apoptosis as measured by TUNEL (Fig. 1*F*).

PEG 15–20 attenuates radiation-induced apoptosis in the intestinal epithelium of mice and radiation-induced mortality following intestinal inoculation with P. aeruginosa. We next determined the effect of 13 Gy abdominal radiation on IEC apoptosis in mice by examining the intestinal segments at 24 h postexposure. In Fig. 2*A*, intestinal segments (ileum) demonstrate morphological changes consistent with radiation injury including a decrease in the number and height of villous projections (villous blunting). In radiated mice drinking a 1% PEG solution, villi appear normal in size and length, similar to unradiated control mice. Apoptosis was analyzed by TUNEL assay and demonstrated no nuclear DNA fragmentation in cross sections from nonradiated mice (Fig. 2*B*) and evidence of apoptosis in irradiated mice. Intestinal epithelial apoptosis was significantly attenuated in mice drinking a 1% PEG 15–20 solution (Fig. 2, *B* and *C*).

As apoptosis was prevented in mice drinking 1% PEG 15–20 following 13 Gy abdominal radiation, we hypothesized that mice would be less vulnerable to postradiation-induced, gut-derived sepsis. To show this, we intestinally inoculated mice with *P. aeruginosa* 24 h following 13 Gy abdominal radiation and followed them for up to 25 days for the development of sepsis and mortality (Fig. 2*D*). Mice drinking 1% PEG 15–20 demonstrated significantly attenuated mortality compared with mice drinking water ($n = 10$, $P < 0.001$) (Fig. 2*E*).

PEG 15–20 suppresses P. aeruginosa expression of the adherence/invasion and epithelial barrier-disrupting virulence protein PA-I lectin/adhesin and repels P. aeruginosa away from the IEC surface. To determine how, under conditions of radiation injury, PEG 15–20 protects the intestinal epithelium against microbial adherence and possible invasion, we first assessed whether soluble compounds are released into the

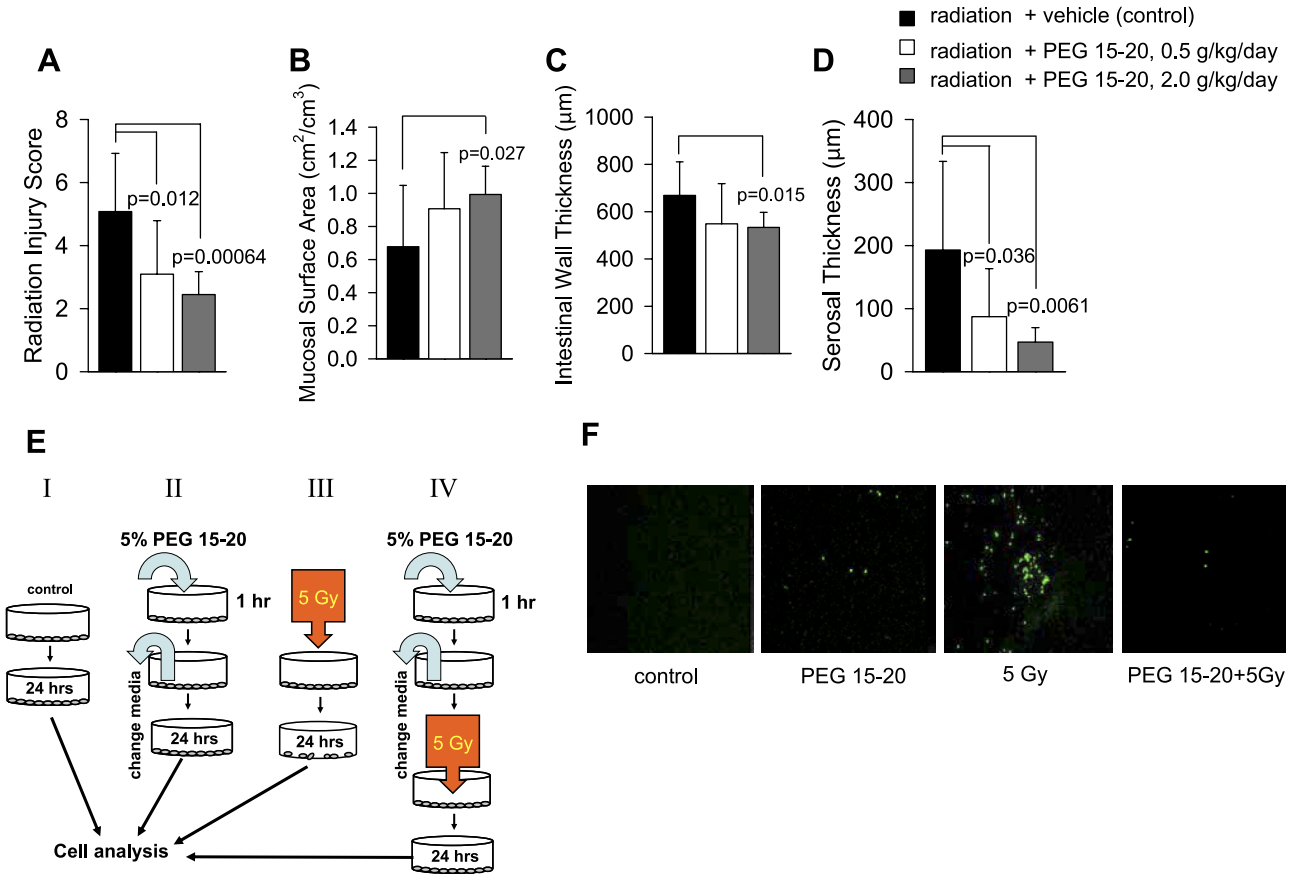

Fig. 1. High-molecular-weight polyethylene glycol 15,000–20,000 Da (PEG 15–20) protects the rat intestine and cultured rat intestinal epithelial cells (IECs) against radiation exposure. *A–D*: dose-dependent protective effect of oral PEG 15–20 on the rat intestine within the scrotum exposed to daily fractionated radiation. Data are means ± SD; $n = 9–12$. *E*: experimental design for cultured rat IECs (IEC-18) exposed to radiation. I: control IEC-18 cells, no treatment. II: PEG-treated cells, IEC-18 cells are exposed to 5% PEG 15–20 for 1 h, followed by gentle washing with culture media, and analyzed in 24 h. III: 5 Gy, IEC-18 cells are exposed to 5 Gy radiation; analysis performed in 24 h. IV: PEG 15–20 + 5 Gy, IEC-18 cells are exposed to 5% PEG 15–20 for 1 h, followed by gentle washing with culture media, and exposed to 5 Gy radiation; analysis performed in 24 h. *F*: nuclear DNA fragmentation detected by TUNEL assay in IEC-18 cells at 24 h posttreatment.

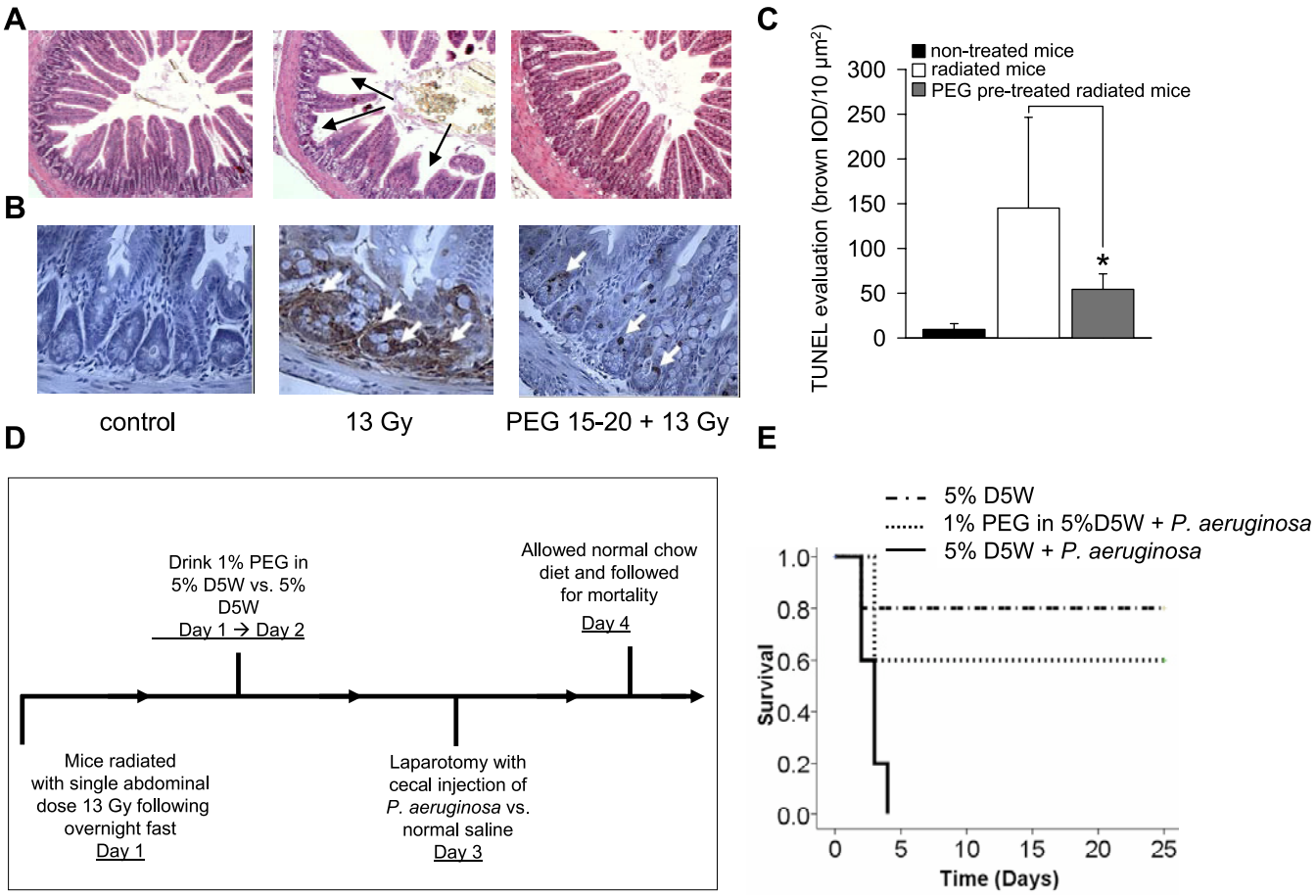

Fig. 2. Mice drinking oral PEG 15–20 are protected against radiation-induced apoptosis and display enhanced resistance to postradiation infection. *A*: Hematoxylin and eosin staining of ileum cross sections demonstrates morphological changes in the intestinal epithelium following abdominal irradiation (13 Gy) with a decrease in the number and height of villous projections (villous blunting, shown by black arrows) that are prevented when mice drink 1% PEG 15–20 (PEG 15–20 + 13 Gy). *B*: TUNEL assay of intestinal epithelial cross sections. White arrows are focused on apoptotic cells. *C*: quantitative assessment of apoptosis performed by measurement of the brown stained area per 10 μm^2 using Automated Cellular Imaging Software, $n = 90$ images from 3 mice/group, $^*P < 0.001$. *D*: experimental design of postradiation infection. *E*: Kaplan-Mayer survival curves demonstrating enhanced resistance against postradiation intestinal exposure to *Pseudomonas aeruginosa* (*P. aeruginosa*) when mice drink oral PEG 15–20 ($n = 10$/group, $P < 0.001$). D5W, 5% dextrose solution in water. IOD, integrated optical density.

apical media of IEC-18 cells following radiation exposure that induce the expression of adherence/invasion and barrier-disrupting proteins in *P. aeruginosa*. We have previously established that expression of the PA-I lectin/adhesin in *P. aeruginosa* plays a critical role in the adherence of this organism to IEC and disruption of tight junctional barrier function, leading to systemic absorption of lethal toxins, sepsis, and death in mice (29). Mutant strains of *P. aeruginosa* lacking the PA-I lectin/adhesin are apathogenic in the mouse intestine (30). Therefore, we exposed the PAO1/*lecA::lux* PA-I lectin reporter strain of *P. aeruginosa* to apical media harvested from IEC-18 cells 24 h following exposure 5 Gy radiation. Results demonstrated a significant increase in PA-I protein expression in *P. aeruginosa* when exposed to media from radiated IEC cells that was attenuated in the presence of PEG 15–20 (Fig. 3*A*). These findings are consistent with our previous work demonstrating that, under conditions of stress (i.e., ischemia, inflammation), IEC secrete soluble compounds that activate the virulence circuitry of *P. aeruginosa* to express a more invasive and lethal phenotype (52). In previous experiments, we demonstrated that human cultured IEC (Caco-2) apically treated with PEG 15–20 exert an electrostatic shielding effect that distances *P. aeruginosa* away from the IEC surface. To determine whether this effect is preserved when IEC cells are exposed to radiation injury in this study, we pretreated cells for 1 h with 5% PEG 15–20 and examined cells for *P. aeruginosa* adherence/invasion following apical inoculation of cells with a GFP-producing *P. aeruginosa* strain PAO1/EGFP (Fig. 3*B*). Results demonstrated that radiation injury accelerates the adherence and possible invasion of *P. aeruginosa* to epithelial cells and that this effect is prevented when cells are pretreated with PEG 15–20 (Fig. 3*B*).

Regional and spatial localization of PEG along the gastrointestinal axis. To determine the distribution and retention characteristics of PEG 15–20 during continuous oral ingestion in mice, PEG 15–20 was labeled with fluorescein, and its distribution and retention characteristics were tracked using in vivo fluorescence imaging (Xenogen). Mice were allowed to drink a 1% solution of Fl-PEG for 7 days. Figure 4*A* depicts in vivo images of mice drinking a control solution containing D5W or a 1% solution of Fl-PEG in D5W on *day 7*. Animals drinking 1% Fl-PEG displayed distribution of the polymer at

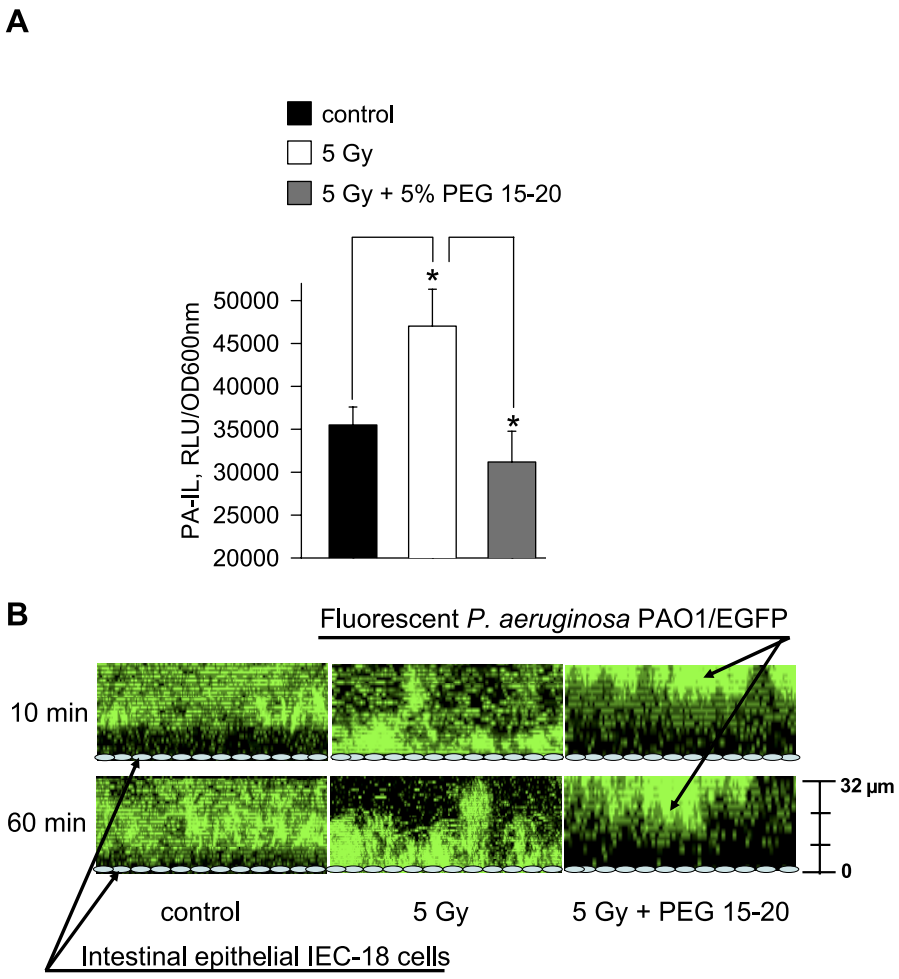

Fig. 3. PEG 15–20 prevents *P. aeruginosa* adherence to and possible invasion of IEC-18 cells and suppresses virulence expression in *P. aeruginosa* when exposed to media from radiated IEC-18 cells. *A*: expression of PA-I lectin/adhesin in *P. aeruginosa* PAO1/lecA::lux exposed to media collected from IEC-18 cells following various treatments. Data represent luminescence values normalized to bacterial cell density (OD 600 nm). PA-I lectin expression is significantly increased in *P. aeruginosa* when exposed to media from irradiated compared with nonradiated cells and significantly decreased when exposed to media from irradiated cells pretreated with PEG 15–20. Data are means ± SD; $n = 4$, $^*P < 0.005$. *B*: *z*-plane reconstructions of multiple stacked images of *P. aeruginosa* PAO1/enhanced green fluorescence protein (EGFP) collected at 10 and 60 min, demonstrating spatial orientation of *P. aeruginosa* to the IEC-18 cell surface. Green fluorescence represents fluorescent *P. aeruginosa* cells. The adhesion/invasion of *P. aeruginosa* to radiated IEC-18 cells is abundant whereby bacteria can be seen suspended above and repelled away from the IEC-18 cell surface when cells were exposed to PEG 15–20 followed by washing with new media. RLU, relative light units.

multiple regions of the gastrointestinal tract including the mouth (pharynx), midgut/hindgut, and within expelled feces. On the basis of the scale bar localized on the right side of the Fig. 4*A*, the luminescence intensity within the intestine of mice drinking D5W is at the expected background level, whereas, in mice drinking 5% dextrose + 1% Fl-PEG, luminescence is significantly increased in the range of $4–8 \times 10^9$ p·s^{-1}·cm^{-2}·sr^{-1}. The same pattern is observed in expelled stool where luminescence intensity in mice drinking D5W is at the level of $\sim 3 \times 10^9$ p·s^{-1}·cm^{-2}·sr^{-1} compared with mice drinking 5% dextrose + 1% Fl-PEG where luminescence is $>8 \times 10^9$ p·s^{-1}·cm^{-2}·sr^{-1}. Images are representative examples of three mice per group. To determine whether the above findings represented the presence of PEG 15–20 on the epithelial surface, we harvested segments of the distal mouse intestine in mice drinking either D5W alone or D5W with PEG 15–20 and determined the height of deflection off the epithelial surface by AFM. Mice drinking PEG 15–20 had a topographically distinct appearance to their mucosal surface (Fig. 4*B*) and a significantly higher height of deflection measurement by AFM (Fig. 4, *B* and *C*).

PEG 15–20 associates within the bilipid membrane. To determine how PEG 15–20 physically interacts within membranes, we performed SAXS using modeled and fully ordered bilipid membranes. PEG 15–20 consists of two monopolymers of Mw 7,000–9,000 linked via an aromatic ring (Fig. 4*D*). The SAXS pattern at 40 ± 2°C displayed two Bragg peaks positioned at q = 0.114 and 0.226 Å^{-1}, indicative of 1-D lamellar (bilayer) stacks with a periodicity of 55.1 Å (Fig. 4*E*). This observation suggests that the PEG 15–20 is associated with the lipid bilayer in such a manner as to direct the two symmetric PEG blocks laterally across the membrane-water interface (not well projected from the surface), yielding a polymer coat across the lipid bilayer. Moreover, the narrow diffraction peaks and the lack of any other features in the SAXS profile suggest the existence of a single phase, meaning that the polymer is, in fact, incorporated into the lipid mixture. Reduction of the sample temperature to 25 ± 2°C caused no observed changes in the corresponding SAXS pattern. Further reducing the sample temperature to 7 ± 1°C caused the pattern to broaden into a single diffraction feature. The observed pattern at reduced temperature indicates that the bisphenol A diglycidyl ether linkage, which serves to couple the two PEG blocks, can insert below the region of the lipid head groups (i.e., into the alkyl chain region) and can therefore anchor the polymer to the membrane as drawn in Fig. 4*F*. The shallow insertion of the bisphenol A diglycidyl ether linkage can cause the constrained PEG blocks to position themselves laterally across the membrane-water interface, an ideal conformational state for barrier formation and protection of the extensive surface area of the intestinal mucosa.

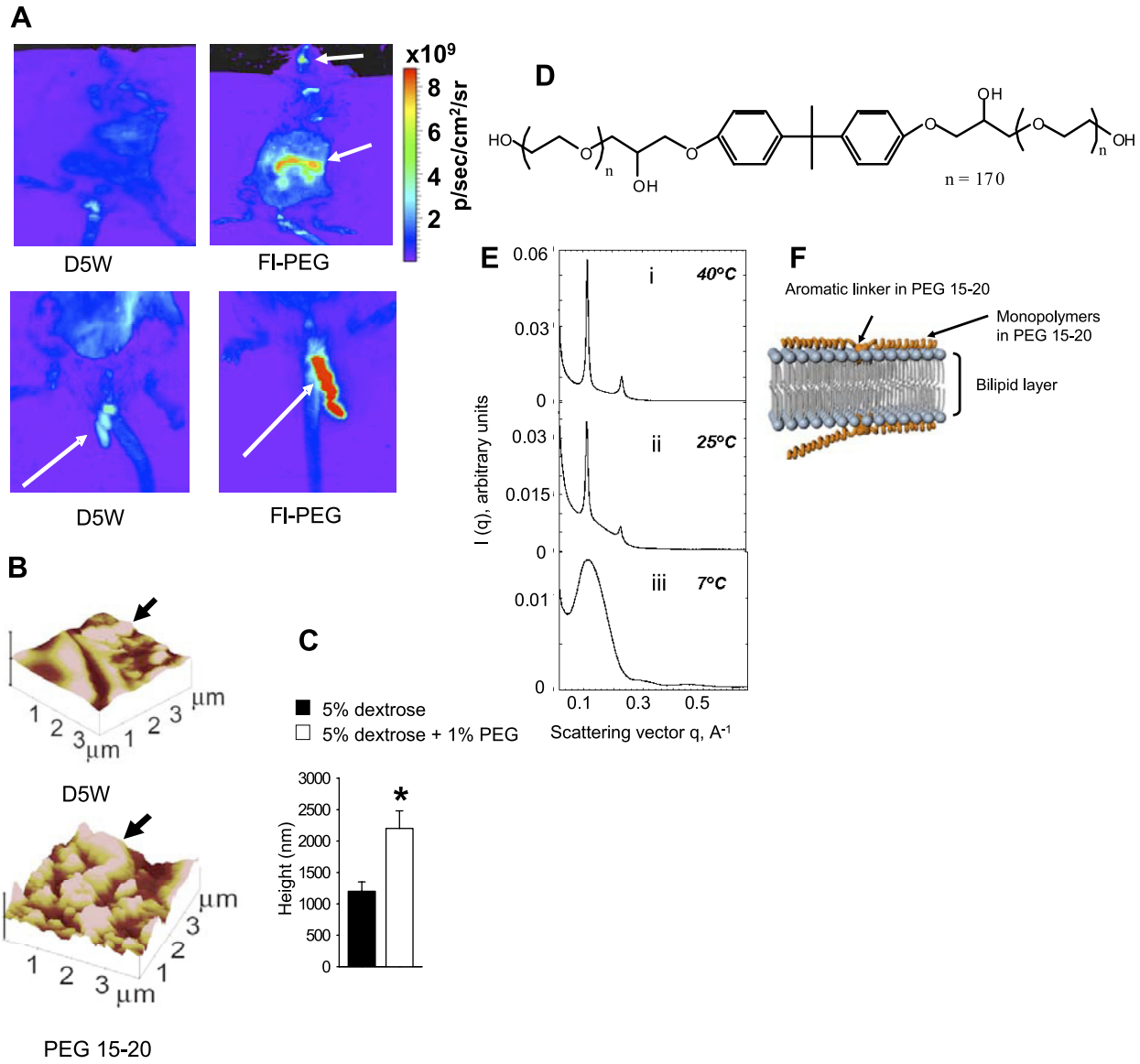

Fig. 4. PEG 15–20 coats the luminal surface of the gastrointestinal tract and associates within bilipid membranes. *A*: Xenogen IVIS 200 images of live mice drinking D5W or 1% fluorescein-labeled PEG 15–20 in D5W (Fl-PEG). *Top*: images of whole mice, arrows on fluorescent spots demonstrating the distribution of the polymer in mouth (pharynx) and midgut/hindgut. *Bottom*: Xenogen images of expelled feces. *B*: atomic force microscopy (AFM) images of midgut segments of intestine of mice drinking D5W (*top*) or 1% PEG 15–20 in D5W (*bottom*). *C*: AFM height deflection measurements; $n = 3$, $^*P < 0.05$. *D*: structure of PEG 15–20. *E*: Synchrotron small-angle X-ray scattering profiles collected at three temperatures, 40°C, 25°C, and 7°C, on samples prepared with PEG 15–20. The quaternary composition consisted of 0.748 weight fraction water, Φ_w; 0.0961 weight fraction dimyristoyl-sn-glycero-3-phosphocholine, Φ_L; 0.1333 weight fraction of polymer, Φ_p; and 0.0221 weight fraction lauryldimethylamine-N-oxide surfactant, Φ_s. q, scattering vector; I(q), the intensity as a function of the magnitude q of the scattering vector. *F*: schematic illustration of PEG 15–20 association with model biological membrane.

PEG 15–20 associates with lipid rafts. To spatially image PEG 15- 20 on live cell membranes, we added 0.25% Fl-PEG to the apical surface of IEC-18 cells for 1 h, washed cells extensively, and then examined them by confocal microscopy. Images displayed in Fig. 5*A* demonstrate the distribution of Fl-PEG on the cell membranes. We next performed sucrose gradient fractionation of IEC-18 cells and found that the Fl-PEG was localized to *fractions 5–9* (Fig. 5*B*) where detergent-resistant domains of the plasma membrane known as lipid rafts are located. To verify that *fractions 5–9* represent lipid rafts, we performed SDS-electrophoresis of these fractions followed by immunoblotting using anti-flotillin antibodies because flotillin is known to be to be enriched on lipid rafts. As seen on Fig. 5*C*, only *fractions 5–9* contained flotillin, confirming that PEG 15–20 was localized to the lipid rafts on IEC-18 cells. To further confirm binding of PEG 15–20 to lipid rafts, we exposed IEC-18 cells to Cholera toxin B, a protein known to specifically bind to lipid rafts. Similar to the above experiments, we pretreated IEC-18 cells with varying concentrations of Fl-PEG for 1 h, followed by extensive washing, then treated cells with Cholera toxin B. We predicted that we would observe colocalization of Cholera toxin B and Fl-PEG to lipid rafts; however, we observed that most of the membranes that were coated with Fl-PEG and did not incorporate toxin B (Fig. 5, *D*, *E*, and *G*), suggesting inhibition of Cholera B toxin binding by PEG 15–20. As seen in Fig. 5*D*, Cholera toxin B

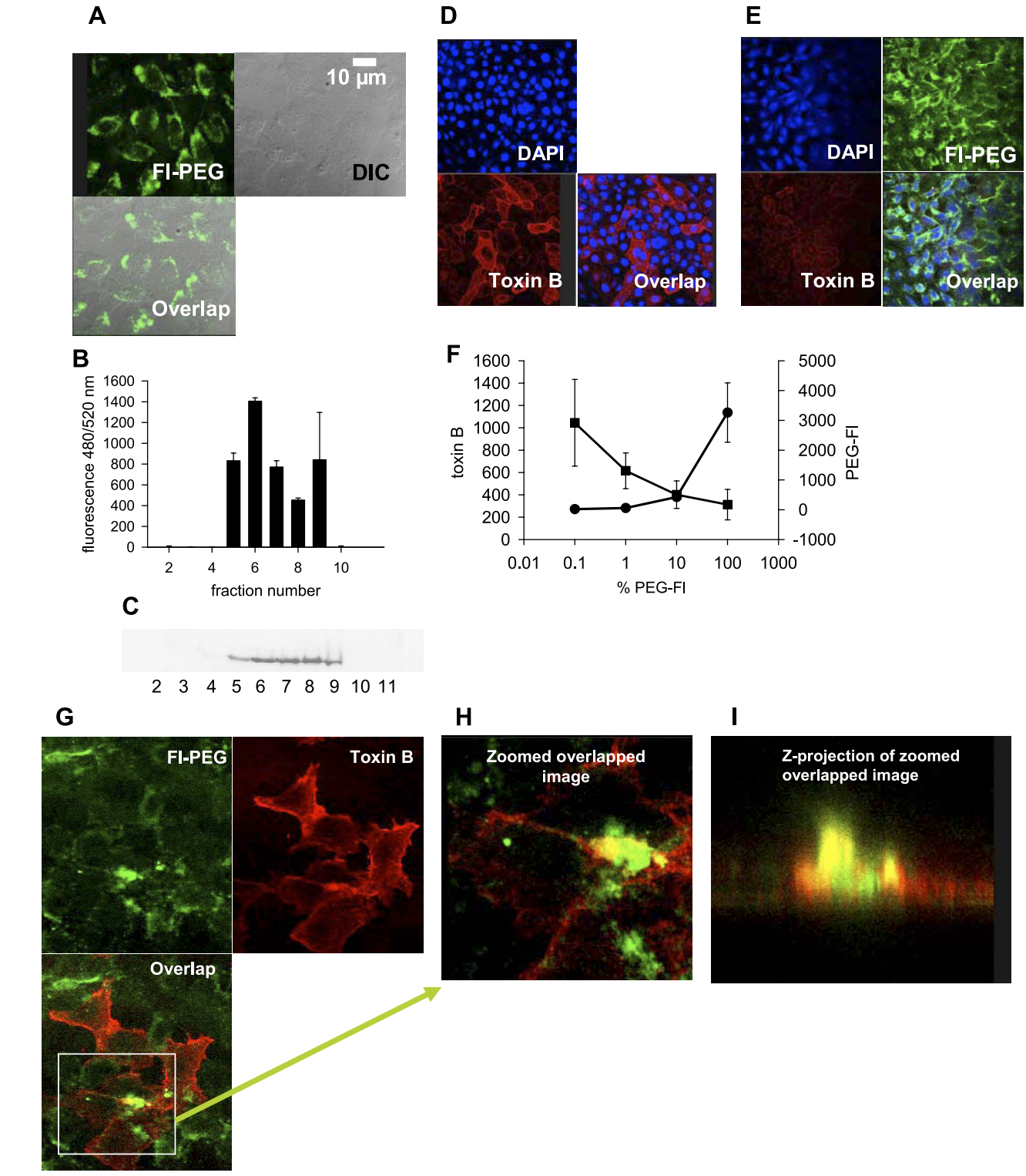

Fig. 5. PEG binds to lipid rafts and competes for binding to lipid rafts with the Cholera toxin B. *A*: image of the IEC-18 cell coincubated with Fl-PEG. *Top*, *left*: fluorescent confocal image. *Top*, *right*: differential interference contrast (DIC) image. *Bottom*: merged image. *B*: fluorescence measured in sucrose gradient fractions of IEC-18 cells coincubated for 1 h with Fl-PEG followed by vigorous washing. *C*: Western blot analysis of sucrose gradient fractions isolated from IEC-18 cells pretreated for 1 h with the Fl-PEG. Purified mouse anti-Flotillin 1 MAb (BD Transduction Laboratories, San Diego, CA) were used in the analysis. *D*: fluorescent confocal images of IEC-18 cells stained with Cholera toxin B to identify lipid rafts. *Top*, *left*: nuclear DAPI staining. *Bottom*, *left*: lipid raft staining using red fluorescent protein-fused Cholera toxin B. *Bottom*, *right*: merged image. *E*: fluorescent confocal images of IEC-18 cells pretreated for 1 h with 0.25% Fl-PEG followed by coincubation with red fluorescent protein fused Cholera toxin B. *Top*, *left*: nuclear DAPI staining. *Top*, *right*: green fluorescence image. *Bottom*, *left*: red fluorescence image. *Bottom*, *right*: merged image. *F*: dose-dependent effect of Fl-PEG on Cholera toxin B binding to lipid rafts. Red fluorescence (toxin B, ■) or green fluorescence (PEG-Fl, ●) intensity were assessed using the Image J program. Data are means ± SD, $n = 10$. *G*: fluorescent confocal images of IEC-18 cells pretreated for 1 h with 0.2% Fl-PEG and stained with Cholera toxin B for the lipid rafts. *Top*, *left*: green fluorescence image. *Bottom*, *left*: red fluorescence image. *Top*, *right*: merged image. *H*: enlarged image of green/red colocalization from *G*. *I*: *z*-plane image of selected area from *H*.

displays ordered localization on cell membranes surrounding nuclei. When IEC-18 cells were, however, preincubated with 0.25% of fluorescent PEG 15–20, the red fluorescence corresponding to Cholera toxin B was significantly attenuated and displaced by green fluorescent Fl-PEG (Fig. 5*E*). We evaluated the intensity of red and green fluorescence attributed to toxin B and Fl-PEG, respectively, and demonstrated a dose-dependent attenuation in the ability of toxin B to bind to lipid rafts in the presence of PEG (Fig. 5*F*). Occasionally, we found areas of colocalization of toxin B and Fl-PEG (Fig. 5, *G* and *H*). Colocalized areas were subjected to *z*-plane imaging and demonstrated that, when PEG associates with lipid rafts, it prevents toxin B binding (Fig. 5*I*). Taken together, these findings suggest that *1*) PEG 15–20 binds to epithelial lipid rafts and *2*) that there is competitive binding of PEG with toxin B. Because *P. aeruginosa* and other important intestinal pathogens are known to alter epithelial barrier function and cellular signaling via their binding to lipid rafts, these data raise the possibility that PEG binding to lipid rafts may play a major role in its protective effect against bacteria invasion and its consequences.

PEG 15–20 prevents coalescence of lipid rafts in IEC-18 cells induced by radiation and P. aeruginosa exposure. Because both radiation and *P. aeruginosa* are known to induce lipid raft coalescence, we examined changes in lipid rafts in IEC-18 cells exposed to radiation injury in the presence and absence of *P. aeruginosa* and in the presence and absence of PEG 15–20. Lipid raft coalescence has been shown to be a specific marker of cellular disruption and a precursor of apoptosis (15, 37). With the use of green fluorescent protein-fused Cholera toxin B, images of lipid rafts in control cells demonstrated a typical distribution of lipid rafts mostly concentrated in the membranes (Fig. 6*A*). Treatment of nonradiated control cells with 5% PEG did not change lipid raft distribution (Fig. 6*B*). However, when epithelial cells were either radiated (5 Gy) (Fig. 6*C*) or exposed to *P. aeruginosa* and 5 Gy radiation (Fig. 6*E*), lipid raft coalescence was observed. Pretreatment with 5% PEG before radiation and exposure to *P. aeruginosa* prevented the observed coalescence (Fig. 6, *D* and *F*).

Depletion of cholesterol abrogates the radioprotective effect of PEG 15–20. Because lipid rafts are known to be rich in cholesterol- and sphingolipid-enriched microdomains and cholesterol is considered to be the dynamic "glue" that holds the rafts together (24), we depleted cholesterol using methyl-B-cyclodextrin (MBC) before exposing the cells to PEG 15–20. After depletion of cholesterol in IEC-18 cells, we repeated experiments where 0.25% Fl-PEG was coincubated with IEC-18 cells. Results demonstrated that cholesterol depletion disrupted the even and ordered distribution of Fl-PEG on cell membranes (Fig. 7*A*). When cholesterol-depleted IEC-18 cells were subjected to 5 Gy radiation, 5% PEG 15–20 did not protect IECs from apoptosis but rather shifted them to display a high degree of necrosis (Fig. 7*B*). Although MBC treatment by itself caused increased necrosis in both nonradiated and radiated cells, preexposure to PEG further increased necrosis in radiated cells, suggesting that the association of PEG 15–20 to lipid rafts plays a predominant role in its protective effect. Finally, we performed reiterative experiments to determine

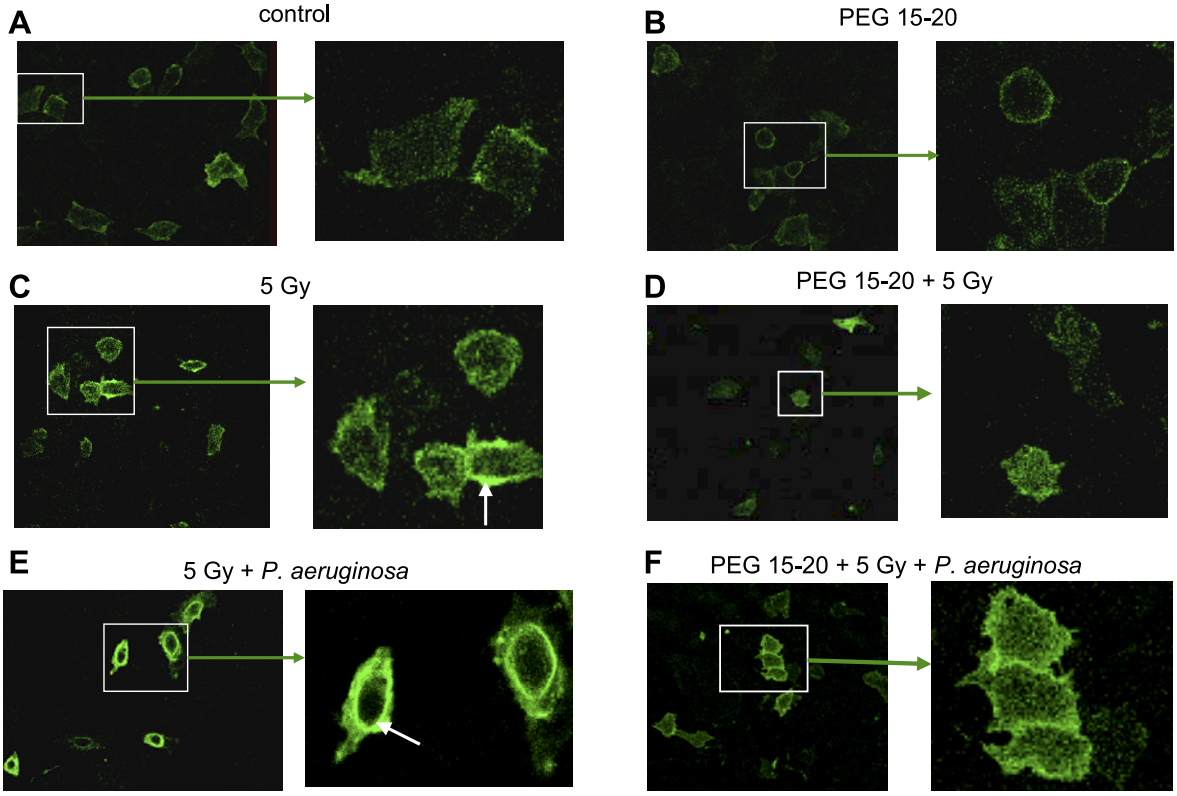

Fig. 6. PEG 15–20 prevents the coalescence of lipid rafts in IEC-18 cells. *A*: control IEC-18 cells. *B*: IEC cells exposed to PEG 15–20 for 1 h. *C*: IEC-18 cells exposed to 5 Gy irradiation. *D*: IEC-18 cells pretreated with PEG 15–20, followed by 5 Gy irradiation. *E*: IEC-18 cells exposed to 5 Gy irradiation followed by infection with *P. aeruginosa* PAO1 for 1 h. *F*: IEC-18 cells pretreated with PEG 15–20, followed by 5 Gy irradiation and infection with *P. aeruginosa* PAO1. White arrows indicate lipid raft coalescence.

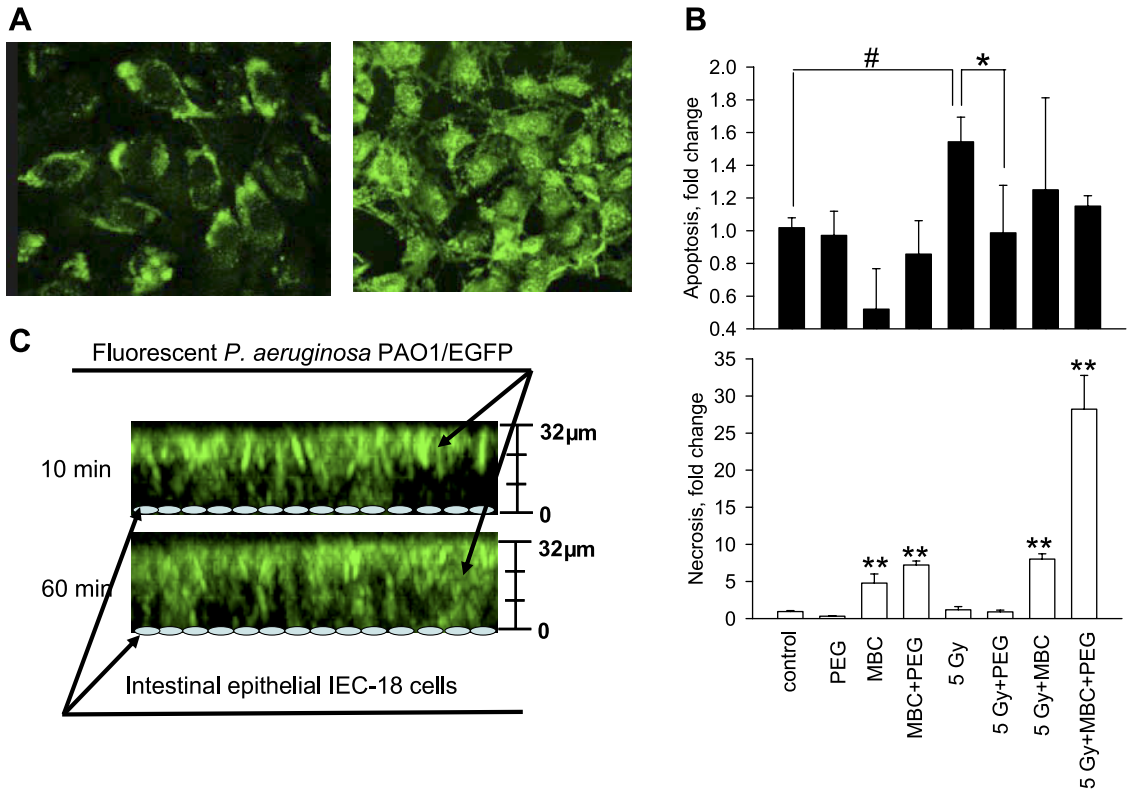

Fig. 7. Methyl-B-cyclodextrin (MBC) treatment of IEC-18 cells abrogates the protective effect of PEG 15–20. *A*: images of IEC-18 cells coincubated with 0.25% Fl-PEG without (*left*) and with (*right*) MBC. *B*: DNA fragmentation (cell death ELISA) measured in IEC-18 cells (apoptosis) and IEC-18 conditioned media (necrosis) ($n = 5$/group, $^*P < 0.005$, $^{**}P < 0.001$). *C*: *z*-plane reconstructions of multiple stacked images of *P. aeruginosa* PAO1/EGFP demonstrating spatial orientation of *P. aeruginosa* to MBC-treated radiated IEC-18 cells. Images demonstrate that depletion of cholesterol attenuates the protective effect of PEG in its ability to repel bacteria away from the intestinal epithelial surface. At 10 min, scattered bacteria are seen attached to IEC-18 cells, which is observed to be more prominent at 60 min.

whether the protective effect of PEG 15–20 against *P. aeruginosa* invasion of radiated IEC-18 cells would be abrogated by cholesterol depletion using MBC. Results demonstrated that PEG 15–20 was not protective against *P. aeruginosa* invasion of radiated IEC-18 cells when cholesterol was depleted by MBC (Fig. 7*C*).

DISCUSSION

In the present study, we demonstrate that PEG 15–20 appears to be an effective agent against the complications of abdominal radiation. During radiation therapy, the intestine is a critical dose-limiting organ in which early and delayed radiation-mediated injury (radiation enteropathy) can develop (49). Early acute radiation enteropathy is characterized by apoptotic cell death in IECs, disruption of the epithelial barrier, and activation of intestinal inflammation. In contrast, chronic radiation enteropathy is characterized by progressive intestinal wall fibrosis and prominent vascular sclerosis. In the present study, we show that both apoptosis and intestinal wall thickening, a surrogate endpoint of fibrosis, can be attenuated by oral PEG 15–20.

A feared complication of abdominal radiation is the development of severe systemic inflammation and sepsis. In this regard, *P. aeruginosa* appears to be especially problematic as a consequence of the radiation effect itself, causing loss of protective (probiotic) and competing bacterial strains. In this regard, the ability of the PEG 15–20 to independently affect both radiation-induced epithelial cell injury and virulence expression and invasion of *P. aeruginosa* may be especially important. The compound used in the present study has been recently shown to protect the intestinal epithelium and mice from colonization and invasion by other Gram-negative bacteria and fungi, and, therefore, its antimicrobial effect may be wider than reported in the present study (19).

That PEG 15–20 may exert its protective effect via lipid raft structural rearrangement and prevention of apoptosis is especially intriguing. Lipid raft coalescence in association with apoptosis is a known sequela of radiation (3, 21). Lipid raft coalescence and induction of apoptosis are also characteristic features of epithelial invasion and infection of *P. aeruginosa*, underscoring the possible synergistic effect of intestinal *P. aeruginosa* following radiation injury (14, 15, 21, 39, 53). One of the major components of lipid rafts is cholesterol that has been hypothesize to represent a type of "dynamic glue" for these structures (24). The role of cholesterol in lipid bilayers is important given the high level of cholesterol in the plasma membrane (~30%) and its influence on the fluid structure and ordering of lipid bilayers (10, 18, 38). Results of the present study that demonstrate that depletion of cholesterol with MBC abrogates ordered binding of PEG 15–20 to IEC-18 cells and its protective effect provide evidence that the protective effect of PEG may require intact lipid raft function.

The effect of PEG on lipid rafts might represent the major mechanism by which it protects the intestinal epithelium

against apoptosis. In response to stress, lipid rafts fuse into larger, more stable signal transduction platforms, resulting in the activation of multiple signaling cascades (25, 42, 45) including the activation of apoptosis. It has been shown that lipid rafts contribute to the bystander induction of apoptosis via signal transduction from cell to cell surface receptors to trigger apoptosis in neighboring cells that are not initially injured by irradiation (15). Because PEG cannot prevent direct DNA damage attributable to radiation exposure, it is likely that the effect of PEG on the development of apoptosis in irradiated cultured IECs and the rodent intestinal epithelium is to contain the propagation of apoptosis in cells injured by radiation, possibly by interrupting cell-to-cell communication signals (i.e., cytokines, paracrine factors) between irradiated and non-irradiated sites.

We have previously reported that, when IECs are injured or ischemic, they release soluble compounds that can activate the virulence circuitry of *P. aeruginosa* to express a barrier-disrupting phenotype (40, 51, 54). We identified a variety of host-derived bacterial signaling compounds released by the intestine in response to injury and stress that induce the expression of multiple virulence determinants in *P. aeruginosa* including pyocyanin and the PA-I lectin. We have previously shown that the PA-I lectin is a critical virulence determinant for lethal gut-derived sepsis in the mouse attributable to *P. aeruginosa* where it causes epithelial cells barrier disruption and the systemic absorption of lethal toxins (29). The PA-I lectin virulence gene is prevalent in clinical strains of *P. aeruginosa* that cause sepsis. Given the ability of PEG 15–20 to affect membrane signaling in intestinal cells, it is possible that PEG also affects bacterial membrane signaling in a manner that modifies its responsiveness to local environmental cues. We have previously shown that PEG 15–20 attenuates the expression of PA-I lectin in *P. aeruginosa* in response to its cognate quorum-sensing signaling molecule C4-HSL(52) and in response to the host proinflammatory cytokine IFN-γ (data not shown). The finding in the present study that PEG 15–20 suppresses PA-I lectin expression in *P. aeruginosa* in response to soluble elements released by radiated IECs might represent yet another mechanism of protection of PEG that occurs via some type of membrane effect. The precise cellular components that are released following epithelial radiation that activate *P. aeruginosa* virulence are under investigation. The inflammatory cytokines TNF-α and IL-1β as well as IL-12 and IL-18, which are secreted and are known to be involved in the inflammatory immune response to ionizing radiation (44), could be considered as potential candidates.

The critical structure of PEG 15–20 that is central to its role and biological function remains to be elucidated (8). SAXS analysis seems to suggest that the PEG 15–20 can anchor and intercalate into the lipid bilayer via its phenol ring. In this manner, flanking PEG chains may cover the epithelium lateral to their anchoring site and thus shield against microbial invasion. Another important property of PEG 15–20 is its ability to distribute along and be retained within the distal intestinal tract, the site where most bacteria densely colonize and cause epithelial disruptions (2, 6, 47). Compounds that will be clinically effective must distribute and be durable at sites where most microbial invasion and epithelial damage occur. Although this can occur anywhere along the axis of the intestinal tract, its wide distribution from oro-pharynx to rectum may offer a particular advantage during radiation therapy.

Finally, toxicity studies with this compound have shown no systemic absorption, diarrhea, or untoward effect on health and growth of animals ingesting large doses over a period of up to 3 wk (data not shown). Therefore, PEGs and related compounds may have clinical value to protect the gut with an acceptable safety profile.

In summary, PEG 15–20 shows significant promise as a radioprotectant with biological properties that may involve lipid rafts. Further work will be necessary to uncover the precise mechanistic details that are responsible for its radioprotective effect.

ACKNOWLEDGMENTS

We thank Stephen P. Diggle, University of Nottingham, Nottingham, UK for providing PAO1/lecA::lux PA-I lectin reporter strain of *P. aeruginosa* and Christine Labno for help with confocal microscopy. We also thank Dr. Rifat Pamukcu for technical advice.

GRANTS

This work was supported by NIH RO1 GM62344-09 (J. C. Alverdy), DDRC grant DK42086 (E. B. Chang), R01 CA83719 (M. Hauer-Jensen), R37 CA71382 (M. Hauer-Jensen), and U19 AI67798 (M. Hauer-Jensen).

DISCLOSURES

Drs. J. Alverdy and E. Chang are founding members of Midway Pharmaceuticals, a polymer therapy company.

REFERENCES

1. **Baddeley AJ, Gundersen HJ, Cruz-Orive LM.** Estimation of surface area from vertical sections. *J Microsc* 142: 259–276, 1986.
2. **Bertz H, Auner HW, Weissinger F, Salwender HJ, Einsele H, Egerer G, Sandherr M, Schuttrumpf S, Sudhoff T, Maschmeyer G.** Antimicrobial therapy of febrile complications after high-dose chemo-/radiotherapy and autologous hematopoietic stem cell transplantation—guidelines of the Infectious Diseases Working Party (AGIHO) of the German Society of Hematology and Oncology (DGHO). *Ann Hematol* 82, *Suppl* 2: S167–S174, 2003.
3. **Bionda C, Hadchity E, Alphonse G, Chapet O, Rousson R, Rodriguez-Lafrasse C, Ardail D.** Radioresistance of human carcinoma cells is correlated to a defect in raft membrane clustering. *Free Radic Biol Med* 43: 681–694, 2007.
4. **Brook I, Elliott TB, Ledney GD, Knudson GB.** Management of postirradiation sepsis. *Mil Med* 167: 105–106, 2002.
5. **Brook I, Elliott TB, Ledney GD, Shoemaker MO, Knudson GB.** Management of postirradiation infection: lessons learned from animal models. *Mil Med* 169: 194–197, 2004.
6. **Brook I, Ledney GD.** Oral ofloxacin therapy of Pseudomonas aeruginosa sepsis in mice after irradiation. *Antimicrob Agents Chemother* 34: 1387–1389, 1990.
7. **Brook I, MacVittie TJ, Walker RI.** Recovery of aerobic and anaerobic bacteria from irradiated mice. *Infect Immun* 46: 270–271, 1984.
8. **Chiang ET, Camp SM, Dudek SM, Brown ME, Usatyuk PV, Zaborina O, Alverdy JC, Garcia JG.** Protective effects of high-molecular weight Polyethylene Glycol (PEG) in human lung endothelial cell barrier regulation: role of actin cytoskeletal rearrangement. *Microvasc Res* 77: 174–186, 2009.
9. **Crawford PA, Gordon JI.** Microbial regulation of intestinal radiosensitivity. *Proc Natl Acad Sci USA* 102: 13254–13259, 2005.
10. **de Meyer F, Smit B.** Effect of cholesterol on the structure of a phospholipid bilayer. *Proc Natl Acad Sci USA* 106: 3654–3658, 2009.
11. **Firestone MA, Seifert S.** Interaction of nonionic PEO-PPO diblock copolymers with lipid bilayers. *Biomacromolecules* 6: 2678–2687, 2005.
12. **Firestone MA, Wolf AC, Seifert S.** Small-angle X-ray scattering study of the interaction of poly(ethylene oxide)-b-poly(propylene oxide)-b-poly(ethylene oxide) triblock copolymers with lipid bilayers. *Biomacromolecules* 4: 1539–1549, 2003.

13. **Geraci JP, Jackson KL, Mariano MS.** The intestinal radiation syndrome: sepsis and endotoxin. *Radiat Res* 101: 442–450, 1985.
14. **Grassme H, Jendrossek V, Riehle A, von Kurthy G, Berger J, Schwarz H, Weller M, Kolesnick R, Gulbins E.** Host defense against Pseudomonas aeruginosa requires ceramide-rich membrane rafts. *Nat Med* 9: 322–330, 2003.
15. **Hamada N, Matsumoto H, Hara T, Kobayashi Y.** Intercellular and intracellular signaling pathways mediating ionizing radiation-induced bystander effects. *J Radiat Res (Tokyo)* 48: 87–95, 2007.
16. **Hammond CW, Ruml DD, Cooper DB, Miller CP.** Studies on susceptibility to infection following ionizing radiation. III. Susceptibility of the intestinal tract to oral inoculation with *Pseudomonas aeruginosa*. *J Exp Med* 102: 403–411, 1955.
17. **Hauer-Jensen M, Poulakos L, Osborne JW.** Effects of accelerated fractionation on radiation injury of the small intestine: a new rat model. *Int J Radiat Oncol Biol Phys* 14: 1205–1212, 1988.
18. **Henderson RM, Edwardson JM, Geisse NA, Saslowsky DE.** Lipid rafts: feeling is believing. *News Physiol Sci* 19: 39–43, 2004.
19. **Henry-Stanley MJ, Wells CL.** Polyethylene glycol influences microbial interactions with intestinal epithelium. *Shock* 31: 390–396, 2009.
20. **Ilangumaran S, Hoessli DC.** Effects of cholesterol depletion by cyclodextrin on the sphingolipid microdomains of the plasma membrane. *Biochem J* 335: 433–440, 1998.
21. **Ipatova OM, Torkhovskaya TI, Zakharova TS, Khalilov EM.** Sphingolipids and cell signaling: involvement in apoptosis and atherogenesis. *Biochemistry (Mosc)* 71: 713–722, 2006.
22. **Jensen MH, Sauer T, Devik F, Nygaard K.** Late changes following single dose roentgen irradiation of rat small intestine. *Acta Radiol Oncol* 22: 299–303, 1983.
23. **Koob AO, Borgens RB.** Polyethylene glycol treatment after traumatic brain injury reduces beta-amyloid precursor protein accumulation in degenerating axons. *J Neurosci Res* 83: 1558–1563, 2006.
24. **Korade Z, Kenworthy AK.** Lipid rafts, cholesterol, and the brain. *Neuropharmacology* 55: 1265–1273, 2008.
25. **Lajoie P, Goetz JG, Dennis JW, Nabi IR.** Lattices, rafts, and scaffolds: domain regulation of receptor signaling at the plasma membrane. *J Cell Biol* 185: 381–385, 2009.
26. **Lamarque D, Tran Van Nhieu J, Breban M.** [What are the gastric modifications induced by acute and chronic Helicobacter pylori infection?]. *Gastroenterol Clin Biol* 27: 391–400, 2003.
27. **Langberg CW, Sauer T, Reitan JB, Hauer-Jensen M.** Relationship between intestinal fibrosis and histopathologic and morphometric changes in consequential and late radiation enteropathy. *Acta Oncol* 35: 81–87, 1996.
28. **Langberg CW, Sauer T, Reitan JB, Hauer-Jensen M.** Tolerance of rat small intestine to localized single dose and fractionated irradiation. *Acta Oncol* 31: 781–787, 1992.
29. **Laughlin RS, Musch MW, Hollbrook CJ, Rocha FM, Chang EB, Alverdy JC.** The key role of Pseudomonas aeruginosa PA-I lectin on experimental gut-derived sepsis. *Ann Surg* 232: 133–142, 2000.
30. **Long J, Zaborina O, Holbrook C, Zaborin A, Alverdy J.** Depletion of intestinal phosphate after operative injury activates the virulence of *P. aeruginosa* causing lethal gut-derived sepsis. *Surgery* 144: 189–197, 2008.
31. **Luo J, Shi R.** Polyethylene glycol inhibits apoptotic cell death following traumatic spinal cord injury. *Brain Res* 1155: 10–16, 2007.
32. **MacNaughton WK.** Review article: new insights into the pathogenesis of radiation-induced intestinal dysfunction. *Aliment Pharmacol Ther* 14: 523–528, 2000.
33. **Maj JG, Paris F, Haimovitz-Friedman A, Venkatraman E, Kolesnick R, Fuks Z.** Microvascular function regulates intestinal crypt response to radiation. *Cancer Res* 63: 4338–4341, 2003.
34. **McBride WH, Mason K, Withers HR, Davis C.** Effect of interleukin 1, inflammation, and surgery on the incidence of adhesion formation and death after abdominal irradiation in mice. *Cancer Res* 49: 169–173, 1989.
35. **Moeser AJ, Nighot PK, Roerig B, Ueno R, Blikslager AT.** Comparison of the chloride channel activator lubiprostone and the oral laxative Polyethylene Glycol 3350 on mucosal barrier repair in ischemic-injured porcine intestine. *World J Gastroenterol* 14: 6012–6017, 2008.
36. **Molla M, Panes J.** Radiation-induced intestinal inflammation. *World J Gastroenterol* 13: 3043–3046, 2007.
37. **Mollinedo F, Gajate C.** Fas/CD95 death receptor and lipid rafts: new targets for apoptosis-directed cancer therapy. *Drug Resist Updat* 9: 51–73, 2006.
38. **Munro S.** Lipid rafts: elusive or illusive? *Cell* 115: 377–388, 2003.
39. **Oskouian B, Saba J.** Sphingosine-1-phosphate metabolism and intestinal tumorigenesis: lipid signaling strikes again. *Cell Cycle* 6: 522–527, 2007.
40. **Patel NJ, Zaborina O, Wu L, Wang Y, Wolfgeher DJ, Valuckaite V, Ciancio MJ, Kohler JE, Shevchenko O, Colgan SP, Chang EB, Turner JR, Alverdy JC.** Recognition of intestinal epithelial HIF-1α activation by *Pseudomonas aeruginosa*. *Am J Physiol Gastrointest Liver Physiol* 292: G134–G142, 2007.
41. **Romanchuk LA, Korshunov VM, Busch W, Ivanov AA, Tarabrina NP.** [The effect of total gnotobiological isolation and antimicrobial preparations on the survival of mice with acute radiation sickness]. *Zh Mikrobiol Epidemiol Immunobiol* 23–25, 1991.
42. **Rotolo JA, Zhang J, Donepudi M, Lee H, Fuks Z, Kolesnick R.** Caspase-dependent and -independent activation of acid sphingomyelinase signaling. *J Biol Chem* 280: 26425–26434, 2005.
43. **Schein PS.** WR-2721: a chemotherapy and radiation-protective agent. *Cancer Invest* 8: 265–266, 1990.
44. **Shan YX, Jin SZ, Liu XD, Liu Y, Liu SZ.** Ionizing radiation stimulates secretion of pro-inflammatory cytokines: dose-response relationship, mechanisms and implications. *Radiat Environ Biophys* 46: 21–29, 2007.
45. **Simons K, Toomre D.** Lipid rafts and signal transduction. *Nat Rev Mol Cell Biol* 1: 31–39, 2000.
46. **Somosy Z, Horvath G, Telbisz A, Rez G, Palfia Z.** Morphological aspects of ionizing radiation response of small intestine. *Micron* 33: 167–178, 2002.
47. **Tascini C, Menichetti F, Stefanelli A, Loni C, Lambelet P.** Clinical efficacy of intravenous colistin therapy in combination with ceftazidime in severe MDR *P. aeruginosa* systemic infections in two haematological patients. *Infez Med* 14: 41–44, 2006.
48. **Teramura Y, Kaneda Y, Totani T, Iwata H.** Behavior of synthetic polymers immobilized on a cell membrane. *Biomaterials* 29: 1345–1355, 2008.
49. **Wang J, Hauer-Jensen M.** Neuroimmune interactions: potential target for mitigating or treating intestinal radiation injury. *Br J Radiol* 80, *Spec No* 1: S41–S48, 2007.
50. **Winzer K, Falconer C, Garber NC, Diggle SP, Camara M, Williams P.** The Pseudomonas aeruginosa lectins PA-IL and PA-IIL are controlled by quorum sensing and by RpoS. *J Bacteriol* 182: 6401–6411, 2000.
51. **Wu L, Estrada O, Zaborina O, Bains M, Shen L, Kohler JE, Patel N, Musch MW, Chang EB, Fu YX, Jacobs MA, Nishimura MI, Hancock RE, Turner JR, Alverdy JC.** Recognition of host immune activation by Pseudomonas aeruginosa. *Science* 309: 774–777, 2005.
52. **Wu L, Zaborina O, Zaborin A, Chang EB, Musch M, Holbrook C, Shapiro J, Turner JR, Wu G, Lee KY, Alverdy JC.** High-molecular-weight polyethylene glycol prevents lethal sepsis due to intestinal *Pseudomonas aeruginosa*. *Gastroenterology* 126: 488–498, 2004.
53. **Yamamoto N, Petroll MW, Cavanagh HD, Jester JV.** Internalization of *Pseudomonas aeruginosa* is mediated by lipid rafts in contact lens-wearing rabbit and cultured human corneal epithelial cells. *Invest Ophthalmol Vis Sci* 46: 1348–1355, 2005.
54. **Zaborina O, Lepine F, Xiao G, Valuckaite V, Chen Y, Li T, Ciancio M, Zaborin A, Petrof EO, Turner JR, Rahme LG, Chang E, Alverdy JC.** Dynorphin activates quorum sensing quinolone signaling in Pseudomonas aeruginosa. *PLoS Pathog* 3: e35, 2007.